JOURNAL OF AIRCRAFT
Vol. 47, No. 3, May–June 2010

Framework for a Landing-Gear Model and Acoustic Prediction

Leonard V. Lopes*
NASA Langley Research Center, Hampton, Virginia 23681
and
Kenneth S. Brentner† and Philip J. Morris‡
Pennsylvania State University, University Park, Pennsylvania 16802

DOI: 10.2514/1.36925

A new system has been developed at Pennsylvania State University for the prediction of landing-gear noise. The system is designed to handle the complex landing-gear geometry of current aircraft, as well as provide predictions for future aircraft landing-gear designs. The gear is represented by a collection of subassemblies and simple components that are modeled using acoustic elements. These acoustic elements are generic but generate noise representative of the physical components on landing gear. The method sums the noise radiation from each component of the landing gear in isolation, accounting for interference with adjacent components through an estimate of the local upstream and downstream flows and turbulence intensities. The acoustic calculations are made using the landing-gear-model-and-acoustic-prediction code, which computes the sound pressure levels at specified observer locations. The method can calculate the noise from the landing gear in isolation or installed on an aircraft for any type of landing gear (main or nose). This paper presents an introduction to the system and initial calibrations by using wind-tunnel experiments and the Aircraft Noise Prediction Program prediction formulas. Noise predictions using the landing-gear model and acoustic prediction are compared with wind-tunnel data for model landing gears of various levels of fidelity and Mach numbers. The initial landing-gear-model-and-acoustic-prediction predictions for dressed configurations show an increase in noise in the frequency range representative of the added landing-gear components. The landing-gear model and acoustic prediction is also compared with wind-tunnel measurements for much larger landing-gear geometry, measured in the Virginia Polytechnic Institute and State University acoustic wind tunnel. Predictions show the ability of the landing-gear model and acoustic prediction to predict the contribution of each component to the overall values. Although the landing-gear model and acoustic prediction is in an early stage of development, the present agreement between the calculations and measurements suggests the method has promise for future application in the prediction of airframe noise.

Nomenclature

A	=	estimated wing surface area
A_r	=	amplitude of reflected sound wave
A_s	=	amplitude of sound wave
B_1	=	cylinder nondimensional shedding function peak shedding variable
B_2	=	cylinder nondimensional shedding function scaling variable
b_w	=	wing span
C	=	length of landing-gear door or chord of wing used in trailing-edge element
C'_d	=	coefficient of drag
C'_l	=	coefficient of lift
c_∞	=	ambient speed of sound
D	=	cylinder diameter
$D(\theta, \phi)$	=	directivity function
d	=	tire diameter
e	=	first cylinder nondimensional spectrum shape variable
F	=	Aircraft Noise Prediction Program spectrum function
F_i	=	loading noise source
$F_{\mathrm{ND}}(S)$	=	nondimensional spectrum function
K	=	Aircraft Noise Prediction Program noise equation constant
k	=	wave number
L	=	landing-gear strut length
L_p	=	sound pressure level
M	=	aircraft Mach number
M_r	=	Mach number in the radiation direction
N	=	number of wheels on landing gear
$\hat{n}$	=	surface normal vector
P_{ij}	=	surface pressure tensor
p	=	second cylinder nondimensional spectrum shape variable
$\langle p^2 \rangle$	=	mean-square acoustic pressure (S, θ, ϕ)
p'	=	acoustic pressure–time history $(\mathbf{x}; t)$
p^*	=	acoustic pressure amplitude at the frequency ω, $(r, \theta, z; \omega)$
r	=	distance from the source to the observer $\lvert\mathbf{x} - \mathbf{y}\rvert$
r_s^*	=	nondimensional distance from source to observer, referenced to b_w
S	=	Strouhal number
$\mathbf{S}$	=	acoustic surface
t	=	time
U_0	=	freestream flow velocity
u_i	=	component of fluid velocity vector
u_0	=	turbulent convection velocity
V	=	volume of flat-plate turbulent region
V_n	=	incident flow velocity
v_i	=	component of surface velocity vector
$\mathbf{x}$	=	observer location
$\mathbf{y}$	=	source location
α	=	turbulent intensity
δ	=	flat-plate turbulent boundary-layer thickness

Received 30 January 2008; revision received 17 November 2009; accepted for publication 18 November 2009.

*Research Aerospace Engineer; leonard.v.lopes@nasa.gov. Member AIAA.
†Associate Professor; ksbrentner@psu.edu. Associate Fellow AIAA.
‡Boeing/A.D. Welliver Professor of Aerospace Engineering; pjm@psu.edu. Fellow AIAA.

ϵ = trailing-edge calibration variable
θ = polar directivity angle, 0 deg front of aircraft and 180 deg behind aircraft
Π^* = nondimensional acoustic power, referenced to $\rho_\infty c_\infty^3 b_w^2$
ρ_∞ = mean atmospheric density
τ^* = Reynolds shear stress
ϕ = azimuthal directivity angle, 0 deg below aircraft and 90 deg to the side

I. Introduction

NOISE has been a major concern in the aircraft industry for many years because of limitations placed on the allowable radiated noise by the Federal Aviation Administration [1] and international standards. Over the past several decades, significant improvement in engine noise reduction has exposed the airframe as a potential primary noise source [2]. On landing, when the aircraft engines are operating at reduced power and the flap system is in a high lift configuration, the airframe can become the major noise contributor [3]. NASA's next-generation aircraft designs ($N+2$ and $N+3$) place the engine above the aircraft in an attempt to scatter the noise from the engines [4]. The scattering caused by the aircraft body attenuates the noise from the engines; therefore, any further reduction in noise levels on the ground must come from the airframe [5].

Airframe noise is caused by any device on the aircraft, excluding the engines, and includes the slats, flaps, vanes, and landing gear [6,7]. Even though each of these noise sources generate sound by different physical mechanisms and have different noise directivity patterns, the noise levels generated may be similar in amplitude [8]. The noise from the flaps, vanes, and slats is characterized by turbulent boundary layers passing over sharp trailing edges [9] and flap-side-edge noise [10]. Trailing-edge noise sources, such as those from the flaps or slats, have been studied extensively [11] and are the focus of ongoing research [12]. The landing gear represent a significant challenge because of the nonuniform flowfield under the wing [13] and the complex landing-gear geometries with small-scale details that affect the high-frequency noise [14]. Interactions between the landing-gear wake and the flap system also contribute to the difficult noise signature [15]. The size and turbulence intensity of the landing-gear wake is very challenging to measure [16] or calculate [17] because of the wake's dependence on landing-gear geometry fidelity, turbulence model, and grid resolution.

Fig. 1 Landing gear installed on Boeing 777.

Landing-gear geometry is composed of bluff bodies with different cross sections, sharp corners, curved hoses, and small fittings. These details make the prediction of the noise from the landing gear different from the other airframe noise sources. None of the various landing-gear components are clean cylinders or airfoils but are connected by flanges, joints, etc., which contribute to a wide range of frequencies in the acoustic signal. Also, small components contribute to the higher frequencies in the range in which human hearing is most sensitive. Very small components, including hoses, nuts, and bolts, can be seen in Fig. 1, which shows landing gear installed on a Boeing 777. Figure 2 demonstrates the difference in noise generated between two landing-gear models: a low- and high-fidelity Boeing 737 scale-model landing gear, tested in the Low Speed Aeroacoustic Facility (LSAF) at The Boeing Company by Stoker [14]. The undressed wind-tunnel model does not include hoses and other small features of the landing gear. Note the difference in levels above the 26th octave band. The detailed flow and acoustic fields of small components, such as wires, hoses, bolts, etc., are nearly impossible to compute directly.

One standard for predicting airframe noise is the airframe noise component of the Aircraft Noise Prediction Program (ANOPP) [18], based on the noise prediction scheme developed by Fink [19]. This method is based on an experimental database of aircraft flight data, as well as wind-tunnel tests by Heller and Dobrzynski [20]. Equation (1) and Table 1 show how the total noise is based on the diameter of the wheels for the truck noise and the length of the oleo for the support strut noise. The support strut assembly includes the oleo and any support struts, as well as any fittings and doors. The truck assembly includes the wheels, the hub caps, and any hydraulic brackets and hoses that might be contained on the truck. The noise directivity is described by an empirical function, which is different for each component. Recent flyover measurements by Stoker [14] have shown that, although the overall sound pressure level is predicted reasonably well by ANOPP, the noise spectrum is underpredicted in the higher frequencies. Because ANOPP relates the noise sources to the properties of only two gross features of the landing gear, it is clearly not suited for the identification of particular landing-gear components or parts of components that are the strongest local noise sources:

$$\langle p^2(S,\,\theta,\,\phi)\rangle = \rho_\infty^2 c_\infty^4 \frac{\Pi^*}{4\pi r^{*2}} \frac{D(\theta,\,\phi)F(S)}{(1-M_\infty\cos\theta)^4} \tag{1}$$

Recently, there has been an attempt by Guo [13] and Guo et al. [21] to categorize the components of the landing gear into three main frequency ranges, depending on their size (namely, very low, low,

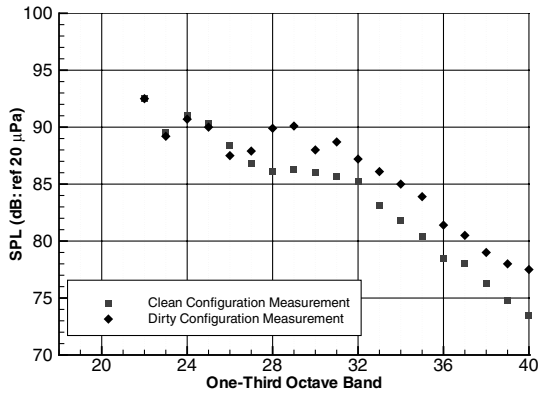

Fig. 2 Measurements of undressed and dressed configuration 737-400 landing gear at a Mach number of 0.20.

Table 1 The acoustic power Π^*, directivity function $D(\theta, \phi)$, and spectrum function $F(S)$ used in ANOPP for the wheel and strut components of a four-wheel landing gear

Sound because of the wheel	Sound because of the strut
$\Pi^*_{\text{wheels}} = K_{\text{wheels}} M_\infty^6 (d/b_w)^2 N$	$\Pi^*_{\text{strut}} = K_{\text{strut}} M_\infty^6 (d/b_w)^2 (L/d)$
$D(\theta, \phi)_{\text{wheels}} = (3/2)\sin^2\theta$	$D(\theta, \phi)_{\text{strut}} = 3\sin^2\theta\sin^2\phi$
$F(S)_{\text{wheels}} = 0.0577S^2(1 + 0.25S^2)^{-1.5}$	$F(S)_{\text{strut}} = 1.280S^3(1.06 + S^2)^{-3}$

and high frequency). This scheme, although predicting each of these frequency ranges, does not provide a direct correspondence of the noise generated to geometrical components of the landing gear.

The present paper describes an alternative approach to the prediction of landing-gear noise, called the landing-gear-model-and-acoustic-prediction (LGMAP) code. LGMAP contains a limited number of simple, generic acoustic elements, which are used to represent the noise generated by geometrically similar parts of very complex landing gear. Each acoustic element can represent a certain type of component on landing gear. Each element applied to a component generates an acoustic signal related to the component's size and its local flow environment. This approach retains the simplicity needed to make the noise prediction problem tractable, yet it has the geometric flexibility needed to model realistic landing gear. It also provides detailed information about how each physical component contributes to the overall radiated noise. Finally, the acoustic elements can be improved, with all the landing-gear components that use that acoustic element benefiting from such an improvement.

This paper is organized as follows. First, the acoustic elements contained in LGMAP are described. Next, the calibration methodology for these elements is explained. After calibration, the ability of the system to predict noise changes because of configuration changes in the landing gear is demonstrated.

II. Approach: Landing-Gear Model and Acoustic Prediction

The central feature of LGMAP is a toolbox of acoustic elements (or objects), as shown in Fig. 3. These include cylinder objects (these can be of any size and any cross section), edge objects (used for door edges, wing flaps, etc.), small fittings, and wheels. These objects are the building blocks that are used to construct the LGMAP representation of any landing-gear configuration. Each object is a simplified geometric representation of the physical component modeled, which uses the local upstream environment as input to predict the noise. In the present implementation of LGMAP, only the freestream flow velocity is used.[§] Engineering judgement is required to determine how to represent the complex landing-gear components in terms of simple LGMAP acoustic elements, but the object geometry is positioned at the correct location within the landing-gear configuration. The upstream environment may include the local flow properties and turbulence levels. The major components of LGMAP will be described in the remainder of this section.

A. Acoustic Element Modeling

The noise from each physical object is modeled with one or more acoustic elements from the acoustic element toolbox. For instance, the oleo, a support strut, and a hose can all be modeled as collections of cylinders. The door and the wing can be modeled as a combination of a reflective surface and a sharp trailing edge. The noise from fittings, nuts, and bolts might be approximated by an additional source. Each of these acoustic elements is explained briefly in this section.

[§]Recent work on this system has incorporated local flow velocity into the prediction system [22]; however, because this paper is introducing only the system, these modification are not presented here.

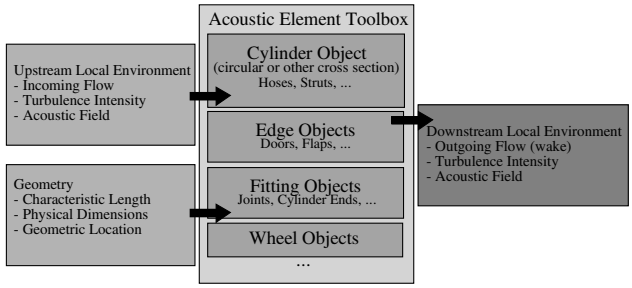

Fig. 3 Schematic of the toolbox of acoustic elements implemented in LGMAP.

1. *Cylinder Element*

The first acoustic element in the toolbox that has been implemented is the cylinder object. This acoustic element can be used to represent many pieces on the landing gear, ranging from the oleo to small hoses. The acoustic radiation by an isolated cylinder is well understood. The cylinder experiences unsteady forces at frequencies dictated by the Reynolds number. In uniform flow, the cylinder experiences unsteady lift and drag forces, which are somewhat different for different cylinder cross-sectional shapes. Cylinder acoustic elements in the LGMAP model are not intended to represent an isolated cylinder but to account for the turbulent environment expected in the vicinity of the landing gear. Thus, the loading for the cylinder is modeled as broadband with a distinct peak at the nominal shedding frequency of an isolated cylinder. A broadband loading spectrum on the cylinderlike components of the landing gear can also account for the fact that the physical landing-gear components are typically not smooth, nor do they have a constant cross section in the spanwise direction.

The unsteady loading on components is the primary source of noise generation for landing-gear geometry. Ideally, a loading noise prediction requires the unsteady surface pressure as input, but for low-frequency noise typical of the unsteady loading on a cylinder, the acoustic wavelength is large compared with the cylinder cross section. Hence, the cylinder can be assumed to be compact in the chordwise (cross-sectional) direction. Therefore, rather than cylinder surface pressures, the loading force as a function of cylinder span can be used as input for the loading noise prediction. The unsteady loads on each cylinder element of the landing gear are modeled using a universal nondimensional loading spectrum. This spectrum is assumed to have a peak frequency S_0, which is representative of the shedding Strouhal number for a cylinder in turbulent flow. The dimensional shedding frequency and the dimensional fluctuating lift and drag forces are determined by scaling the loading for each cylinder element, using the normal component of the local environment velocity. The presence of incoming turbulence or nonuniformity in the cross section is not modeled explicitly but rather incorporated indirectly by broadening the loading spectrum. The nondimensional loading spectrum function is given by

$$F_{\text{ND}}(S) = B_2 S^{e-1}(B_1 + S^p)^{-e} \tag{2}$$

$$B_1 = -S_0^p\left(\frac{e(1-p)-1}{e-1}\right); \qquad B_2 = \left[\int_S S^{e-1}(B_1 + S^p)^{-e}\right]^{-1} \tag{3}$$

$$L'(S) = \tfrac{1}{2}\rho V_n^2 D C_l' F_{\text{ND}}(S); \qquad D'(S) = \tfrac{1}{2}\rho V_n^2 D C_d' F_{\text{ND}}(2S) \tag{4}$$

This nondimensional spectrum is used as a universal cylinder spectrum for all cylinder elements. The peak frequency S_0, the spectral shape (governed by the parameters e and p), and the fluctuating lift and drag coefficients, C_l' and C_d', respectively, can be varied on the basis of the cross-sectional shape, element location, etc. In this way, there can be several classes of cylinder elements. Two such choices of nondimensional loading spectrum are shown in Fig. 4.

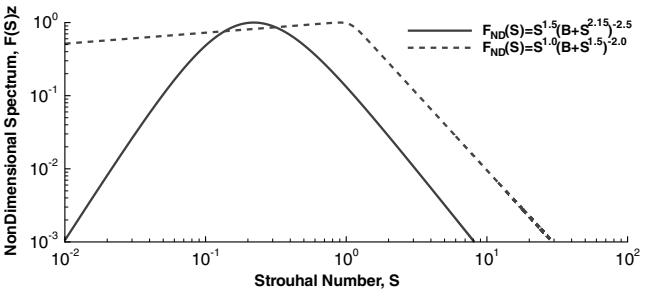

Fig. 4 Typical loading spectra for a cylinder acoustic element: $F_{ND}(S)$ (multiplied by A^{-1} for ease of comparison), the solid line has a peak value of $S_0 = 0.22$, and the dashed line has a peak Strouhal number of $S_0 = 1.0$.

In principle, the parameters used in the nondimensional spectrum could be determined from available measurements or computations. One potential source for guidance is the extensive collection of cylinder data found in Zdravkovich [23,24]. However, it would not be appropriate to use the unsteady force coefficient data for a smooth-surface cylinder in a low-Reynolds-number and low-turbulence environment. Instead, the values have been determined by calibration of the complete noise prediction with experiments. Interestingly, the fluctuating lift and drag values found in this manner are reasonably close to the values reported by Zdravkovich. As further calibrations of the model are performed, it is expected that fluctuating force values for turbulent flows will be somewhat greater than for smooth low-Reynolds-number flows.

One of the useful features of the present methodology is the ability to calibrate the model via experimental measurements. It is anticipated that such a calibration would only be performed once in the development of each cylinder type (i.e., by adjusting e and p) and then used for all subsequent landing-gear noise predictions.

In Fig. 5, the parameter e is varied to show its effect on the nondimensional loading spectrum. As the parameter e is increased, the amplitude at lower frequencies is decreased, but the level in the midfrequency range is increased to keep the integral of the loading function equal to unity. Keeping the integral equal to unity ensures

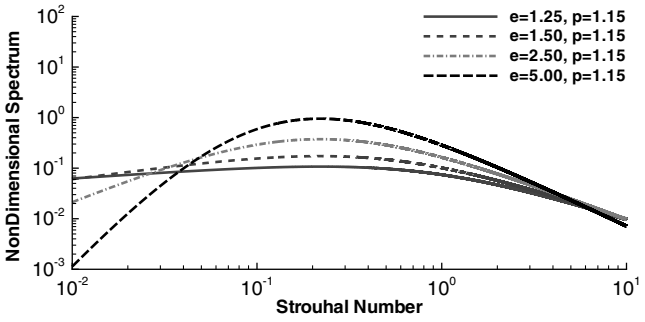

Fig. 5 Effect of the parameter e on the nondimensional spectrum function $F_{ND}(S)$: as e increases, the spectrum at lower frequencies is reduced, but the peak value increases.

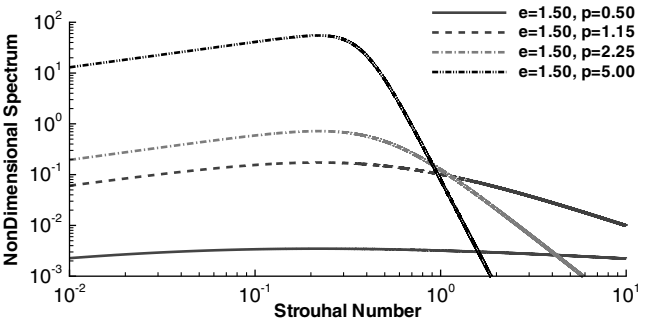

Fig. 6 Effect of the parameter p on the nondimensional spectrum function $F_{ND}(S)$: as p increases, the spectrum at higher frequencies is reduced, but the peak value increases.

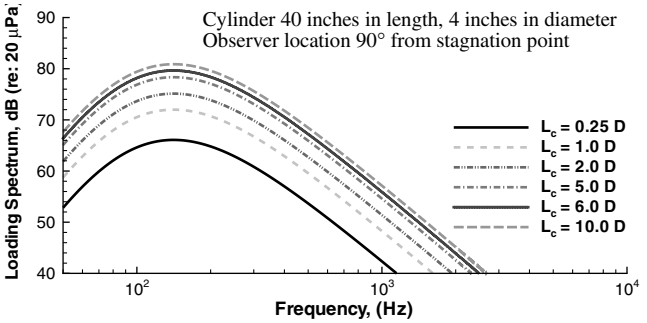

Fig. 7 Variation of the SPL as a function of spanwise correlation length L_c: cylinder overall length equals 40 in., cylinder diameter equals 4 in., and $V_n = 65$ m/s.

the actual levels are controlled by the global parameters, such as V_n and D alone. Similarly, in Fig. 6, the variable p is increased to show how the higher-frequency portion of the loading spectrum can be damped. In this case, the low-frequency and midfrequency levels increase with increasing p.

Another parameter in the cylinder model is the correlation length L_c. It is assumed that, after only a short spanwise distance, the loading is no longer correlated. This distance is a function of wavelength; however, in the noise computation, each cylinder is divided into segments equal to the spanwise correlation length L_c, which is the spanwise distance over which the loading of all frequencies is assumed to be correlated. In future implementations, this may be changed. The LGMAP model currently assumes that all cylinder segments are uncorrelated from all other acoustic elements, as well as other segments of the cylinder under consideration.¶ In Fig. 7, the correlation length is varied for a 0.1-m-long cylinder with 0.01 m diameter exposed to a uniform upstream flow of 65 m/s. The correlation length is changed from half a diameter to 10 diameters, which is the entire length in this case. The noise continues to increase, because the loading is assumed to be perfectly correlated over this length and uncorrelated over all others. As the figure shows, as the correlation length increases, so does the noise. This shows that the assumed correlation length is an important parameter in this model, which has the effect of adjusting the overall level of the noise. But it should be stressed again that, like the other parameters, L_c is not expected to change greatly in subsequent landing-gear noise predictions after its initial calibration.

2. *Wheel Element*

The wheels on landing gear are large physical components, but they also contain small details and have a complex flowfield around them. The small details, such as the tire tread and hub caps, generate turbulence, which is convected downstream to the next wheel. The wake from the first wheel interacts with the second and so on. This has been shown to significantly dampen the primary low-frequency (large-object) shedding and generate a more broadband signal. Furthermore, the wheels generate noise that radiates to the side and downward. Therefore, to accurately predict the noise from the wheels, the acoustic model for the wheel needs to account for all these features.

In LGMAP, the wheel is represented by a ring of cylinder segments. The ring has a diameter equal to the tire diameter, and each cylinder segment in the ring has a diameter equal to the tire width. Figure 8 shows several views of a wire frame drawing of the wheel model. The main reason for using a circle to represent the wheel is that noise is radiated both downward and to the side. The importance of sideline noise was noted by Crighton [6] in his review of the earlier work of Heller and Dobrzynski [20]. Although the flow around a tire has little similarity to flow around a cylindrical ring, this model was chosen because, with suitable calibration, it will provide a first estimate to noise radiation that is representative of a real wheel. It is also important to note that the cylinder segments used to make up the

¶This aspect of the LGMAP model could be changed in the future.

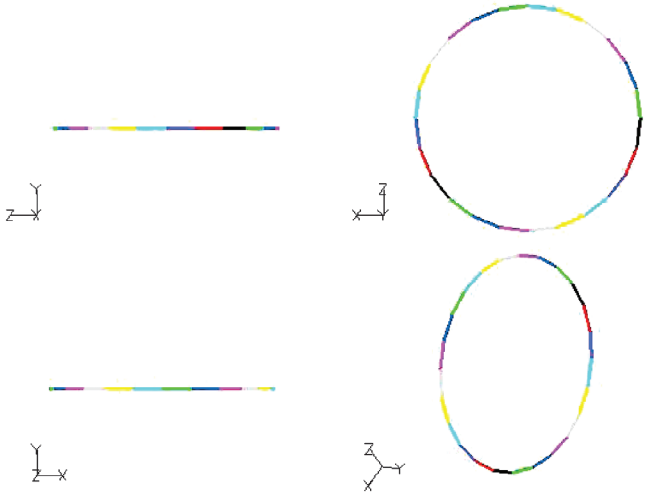

Fig. 8 The geometry of the current wheel acoustic element at different angles: each cylinder implemented in the wheel acoustic element is shown as a different color.

wheel ring use a different loading spectrum than ordinary cylinder elements. The spectrum and corresponding forces on each cylinder have been chosen so that this wheel model will have the same peak shedding frequency found in the ANOPP formula.

The present wheel model is considered crude; hence, more work is needed to refine the wheel model. In the future, alternative wheel models will be developed to better represent the noise generated by the wheels, especially at the higher frequencies. For instance, surface pressure data from a computational fluid dynamics (CFD) simulation of an experiment could be used to resolve the hub, which includes small surface features adding to higher frequencies. Also, small features, such as tire treads, are expected to contribute to the noise at higher frequencies.

3. *Trailing-Edge Element*

In installed landing gear, an important noise source may be from interactions between the landing-gear wake and the trailing edge of the wing and/or flaps. However, in uninstalled landing gear, the wing is not included. The primary sharp edge in uninstalled geometry is from the trailing edge of the landing-gear door (if a door is present). The length of the door trailing edge is relatively small, compared with the wing, but the flow in this region typically contains many small turbulent eddy-generating structures. Even though the landing-gear door is significantly different from the wing, both structures generate noise by the same mechanism; thus, one scalable acoustic model can be used.

The equation for the far-field acoustic spectrum, because of sources in the vicinity of a sharp edge, is given by Ffowcs Williams and Hall [9]:

$$4\pi p^*(r,\ \theta,\ \phi;\ \omega) = \frac{2^{5/2}}{\pi^{1/2}} \frac{e^{i[(1/4)\pi - kr]}}{r} k^{1/2} \sin^{1/2}\phi \cos\tfrac{\theta}{2} \tau^* \delta^{-3/2} V \quad (5)$$

The Reynolds shear-stress term can be modeled using the turbulence intensity α [25–27] and some spectrum function $F(s)$, which is dependent on the turbulence Strouhal number:

$$\tau^* \approx F(S)\rho_0 u_0^2 \approx F(S)\rho_0 \left(\frac{u_0}{U_0}\right)^2 U_0^2 = F(S)\rho_0 \alpha^2 U_0^2 \quad (6)$$

V is the volume of the turbulent source region, which can be estimated to be $\epsilon\delta A$, where A is the estimated plate area, δ is the thickness of the turbulent field, and ϵ is an arbitrary constant of order $\mathcal{O}(1)$. Next,

$$4\pi p^*(r,\ \theta,\ z;\ \omega) = \epsilon \frac{2^{5/2}}{\pi^{1/2}} A \rho_0 U_0^2 \alpha^2 \delta^{-1/2} k^{1/2} F(s) \frac{e^{i[(1/4)\pi - kR]}}{R} \sin^{\frac{1}{2}}\phi \cos\frac{\theta}{2} \quad (7)$$

The directivity function for a trailing edge is different from that of a circular cylinder: θ is defined as the angle between the upstream flow direction and the radiation vector, and ϕ is defined as the angle between the spanwise direction of the trailing edge and the radiation vector. Figures 9 and 10 show how the following function,

$$D = \sin^{1/2}\phi \cos\frac{\theta}{2}$$

varies according to these two parameters. This is the model that is used for the noise from a trailing-edge acoustic element. At this stage of development, only three things need to be modeled: the turbulent intensity $\alpha \approx 0.1$, the nondimensional turbulent spectrum $F(S)$, and the thickness of the turbulent region δ.

To predict the spectrum of surface pressure near the trailing edge, the ANOPP trailing-edge acoustic spectrum, as shown in Eq. (8),

$$F(S) = 0.613(10S)^4[0.5 + (10S)^{1.5}]^{-4} \quad (8)$$

is used as a starting point. However, similar to the wheel and cylinder acoustic elements, this will be recalibrated, as described in Sec. III.

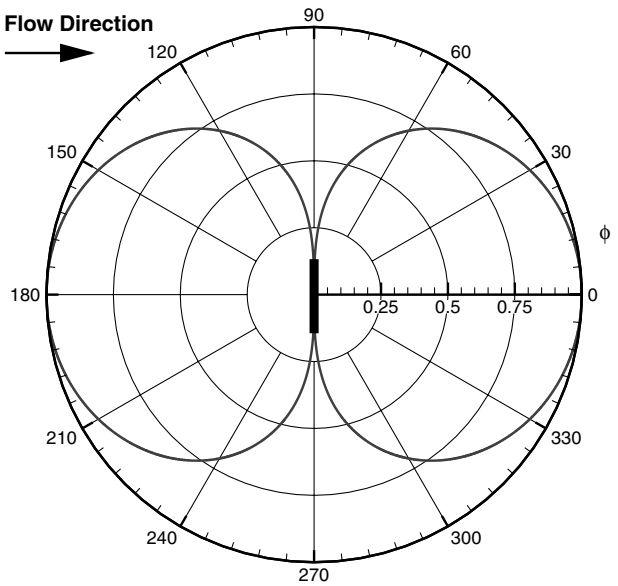

Fig. 9 Directivity of trailing-edge source: flow is from left to right, and edge is from top to bottom.

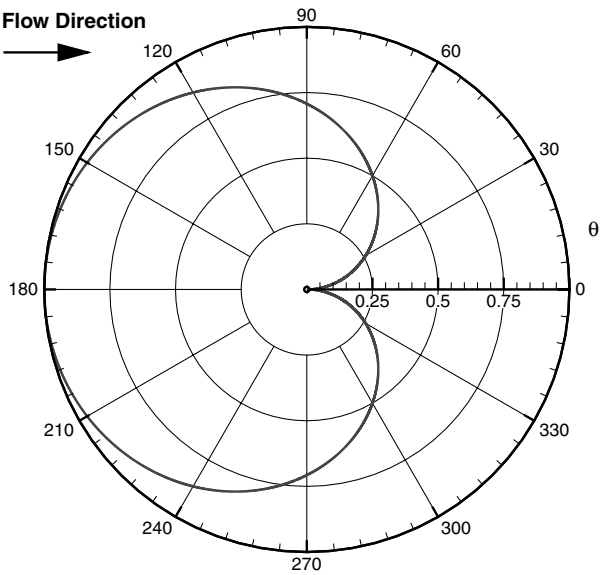

Fig. 10 Directivity of trailing-edge source: flow is from left to right, and edge is out of page.

In the following subsection, the component interaction between the acoustic elements is described.

B. Component Interaction

The geometry of the landing gear, which includes many components of varying sizes in close proximity, represents a challenge when accounting for interactions between components. These interactions include both flowfield interactions (e.g., wakes from an upstream component interacting with a downstream component) and acoustic interactions (e.g., large components scattering and shielding the noise generated by the smaller components behind them and the reflection of acoustic signals off of large objects, such as the wing of the aircraft or a wind-tunnel wall). The next few subsections describe how the LGMAP methodology could handle the interactions between landing-gear components.

1. Flow Interactions

Because the landing-gear geometry has many parts of varying sizes, upstream components can have a strong influence on downstream components. Some of these influences include the change in direction and magnitude of the local flow velocity and an increase in turbulence level experienced by a downstream component. These interactions can be included in the LGMAP model through simple mechanisms. These simple mechanisms provide the interface between higher-order computations or other estimates of the local flow and the LGMAP prediction system. This can be accomplished by modifying the upstream environment of the downstream component to include the upstream component's influence.

The upstream environment includes the local flow velocity, the incoming turbulence level, and an incident acoustic field. The local flow velocity is important when considering small-scale components adjacent to larger-scale parts, large-scale components generating wakes (which convect into small components), the wing boundary layer interacting with the landing gear, or other related flowfield phenomena. The incoming turbulence level potentially affects the loading spectrum and loading level on the component. The incident acoustic field may be shielded by the component. Although all of these affects may potentially be important factors and will be included in future implementation of the LGMAP framework, the current implementation uses only the freestream flow velocity as input into the acoustic elements.

2. Acoustic Interactions

In landing-gear configuration, there is a large range of component sizes and a related range of acoustic wavelengths. Although, in the current implementation, acoustic elements have no direct interaction and, clearly, the acoustic field from some components can be strongly affected by other components. In particular, it would be expected that, when a small component radiates sound at short wavelengths, a larger object will scatter the sound field. In fact, depending on the relative size and spatial relationship, the acoustic signal from one component could be completely shielded by another component, with the result that the small component would not contribute to the total acoustic field at some observer locations.

A full prediction of acoustic scattering will be difficult to implement because of the complex geometry of the landing gear. Initial modeling will focus on shielding (depending on the relative size and proximity of components). The initial implementation of acoustic interactions in the LGMAP model will assume that only components with a direct line of sight will contribute to the acoustic signal at an observer location. A simple variation of this can approximate a scattered field: that is, a fraction of the noise from shielded components might be assumed to reach the observer.

3. Wall Reflections

When comparing the LGMAP predictions with flight-test measurements or wind-tunnel data, it is important to account for all possible sound sources. For an installed landing gear, the noise generated by the landing gear might be reflected from the wing and radiated downward toward a microphone location. In a wind tunnel, the sound generated by the landing gear can be reflected off the tunnel walls. Even though the reflections off a wing or a tunnel wall depend on wavelength, an initial estimate of acoustic reflection can be approximated by a perfectly reflecting infinite wall. The most widely used method for wall reflection is to add an image source system to the noise prediction, as shown in Fig. 11. An alternative approach to compute the noise at an image observer location and then to add it to the original signal, as shown in Fig. 12, was found to be identical to the more traditional method and required less memory and computation time; therefore, it is implemented in LGMAP.

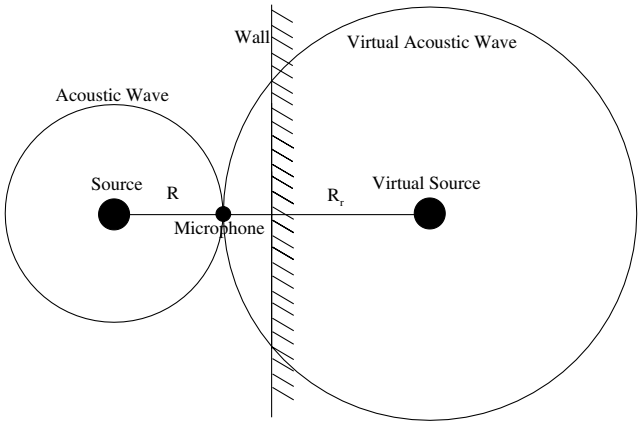

Fig. 11 Schematic showing the virtual source located at a different distance and orientation from the observer than the nonreflected source; the difference in noise can be computed from the distance of the observer to the wall.

The acoustic pressure at the actual observer without the reflected signal is defined as

$$p'_s(\mathbf{x}, \omega) = A_s e^{-i\omega t} \tag{9}$$

where p'_s is the acoustic pressure from the source located at $\mathbf{x}$, and A_s is the amplitude of that signal at the frequency ω. The acoustic pressure from the reflection p'_r is defined as a different source strength A_r plus a time offset Δt, as shown in the following equation,

$$p'_r(\mathbf{x}, \omega) = A_r e^{-i\omega(t+\Delta t)} \tag{10}$$

where Δt is the time offset, which can be found from the geometry of the source, observer, and wall (as shown in Fig. 12) and is defined as $\Delta t = (R_r - R)/c_\infty$. Thus, the total noise from the source with the reflection is

$$p'(\omega) = (A_s + A_r e^{-i\omega\Delta t})e^{-i\omega t} \tag{11}$$

This can be interpreted as an overlaid oscillatory signal in the frequency domain of frequency $\omega\Delta t$ and amplitude A_r. Figure 13

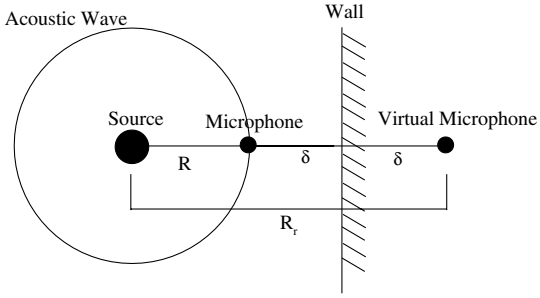

Fig. 12 Schematic showing the virtual observer at a farther distance from the source than the actual observer; the difference in the noise can be calculated by the time offset $\Delta t = (R - R_r)/c_\infty$, which can be used to calculate a phase difference per frequency of $\omega\Delta t$.

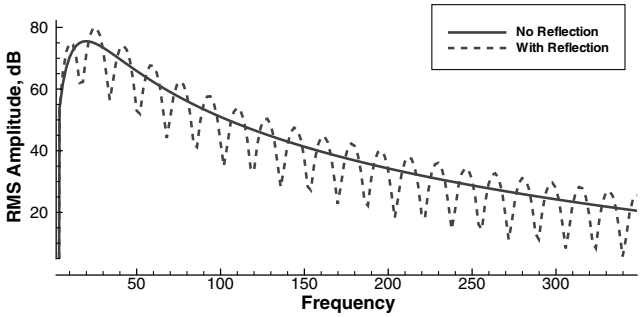

Fig. 13 Noise from isolated source compared with source plus wall reflection; wall reflection adds overlaid oscillatory signal to isolated condition.

shows a 1 Hz bin width result compared with this analytical solution for a simple cylinder in the vicinity of a wall.

C. Acoustic Calculations

The noise prediction is performed using the LGMAP code, which is an extension of PSU-WOPWOP code [28,29]. LGMAP uses an object-oriented design implemented in FORTRAN 95. As such, it is a general-purpose acoustics prediction code. The code uses a source-time dominant algorithm to compute the radiated noise at an arbitrary observer location using Farassat's formulation 1A, which is an integral representation to the solution of the Ffowcs Williams–Hawkings equation [30]. Equation (12) is the loading term of formulation 1A, which can be shown to be the primary noise source type for landing gear,

$$4\pi p'(\mathbf{x}, t) = \frac{1}{c_\infty}\int_{f=0}\left[\frac{\dot{F}_r}{r|1-M_r|^2}\right]_{\text{ret}} \mathrm{d}\mathbf{S} + \int_{f=0}\left[\frac{F_r - F_M}{r^2|1-M_r|^2}\right]_{\text{ret}} \mathrm{d}\mathbf{S} + \frac{1}{c_\infty}\int_{f=0}\left[\frac{F_r(r\dot{M}_r + c_\infty M_r - c_\infty M^2)}{r^2|1-M_r|^3}\right]_{\text{ret}} \mathrm{d}\mathbf{S} \tag{12}$$

where

$$F_i = P_{ij}\hat{n}_j + \rho u_i(u_n - v_n) \tag{13}$$

It is assumed that, for each element having a spanwise length many times greater than its diameter, the spanwise correlation length is of the order of its diameter. The precise correlation length is an input parameter. This is plausible for all components in a turbulent flow. Thus, at the peak frequency of the loading spectrum and lower frequencies, the source can be considered to be acoustically compact with regard to the element's cross section. Elements that are longer than the correlation length are automatically divided into segments in the acoustic computation. The ability of the code to use a compact cross-sectional loading model significantly reduces the amount of data needed for each of the segments. The computed noise from each element is added together, assuming that the component sources are uncorrelated.

III. Calibration

In the current version of the code, the parameters are calibrated by comparing the predicted results with wind-tunnel tests. Next, the model is compared with other measurements to give an estimate of the accuracy of the model. During this development, several different landing-gear geometries were used, ranging from a simple configuration representative of a DC-10 nose gear to a much more complex semidressed Boeing 777 main gear.

In the wind-tunnel test of Heller and Dobrzynski [20], the sideline noise, which is mostly composed of noise from the support strut assembly, is reported for a model representative of a DC-10 nose gear. The support strut assembly contains the oleo and several other struts that are modeled as cylinders in LGMAP. The Heller and Dobrzynski test is used to calibrate the cylinder model. Also, the noise contribution from the doors, modeled as a combination of reflective surfaces and sharp trailing edges in LGMAP, is reported. Although the LGMAP trailing-edge model is still in its early stages of development, the Heller and Dobrzynski wind-tunnel measurements of the door are used for calibration.

Table 2 Parameters used in the cylinder model

	e	p	S_0	C'_l	C'_d
Starting cylinder element model	3.0	2.0	0.22	1.0	0.5
Calibrated cylinder element model	2.5	2.15	0.22	0.17	0.085

An ANOPP calculation is used to calibrate the wheel model. Although it is understood that ANOPP predicts overall levels well, it does not predict the spectrum shape accurately. Even so, the ANOPP wheel model is used for calibration, because it has the ability to predict the isolated wheel noise. Also, ANOPP can predict the noise at any observer position, including below the landing gear, where wheel noise is significant.

When calibrating either the cylinder or wheel acoustic element models, the fluctuating lift and drag coefficients, along with peak Strouhal number for a Reynolds number of 500,000 (as found in Zdravkovich [23,24]), are used as the starting point. These values are only appropriate for smooth cylinders with minimal upstream turbulence; hence, they must be adjusted to account for the expected turbulence in the vicinity of the undercarriage and for the surface nonuniformity found in realistic landing gear. The ultimate effect of upstream turbulence and surface roughness is a broadband loading spectrum acting on the cylinder element. The strut noise spectrum function of four-wheel landing gear from ANOPP is used as the basis for the loading spectrum model for cylinders used in LGMAP. The ANOPP function sets the starting values of e, p, and S_0 in the spectrum function. In the LGMAP model, the rise and falloff rate coefficients e and p in the fluctuating forcing functions for the cylinder are calibrated to match the reported spectrum. The starting values for the cylinder model are shown in Table 2.

A. Cylinder and Trailing-Edge Element

The model DC-10 nose gear experiments were performed at the outdoor wall-jet flow facility located at the DFVLR Trauen test grounds [20]. The nose gear used in the tests did not include all the dressings common in landing gear; hence, the only components that were exposed to the flow were the oleo, a support strut, the doors, and a pair of wheels. The noise from each component was determined in the wind-tunnel test so they could be compared directly with the LGMAP prediction. The measurements for a sideline observer were reported to be dominated by the oleo or strut noise; thus, the data at this observer position have been used to calibrate the spectrum shape

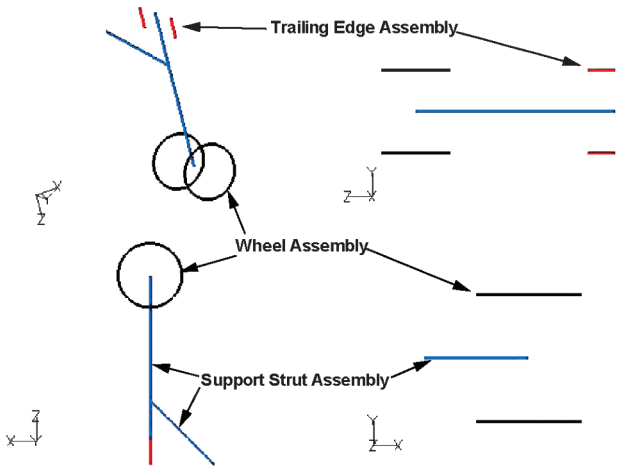

Fig. 14 The LGMAP model for the DC-10 nose gear.

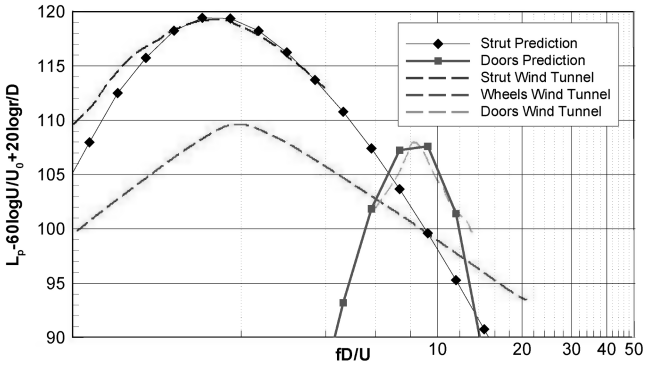

Fig. 15 Comparison of predicted sideline noise with measurements by Heller and Dobrzynski [20]: D is wheel diameter, U is 65 m/s, U_0 is a reference velocity of 100 m/s, f is frequency, and r is observer position.

and the unsteady loading coefficients for the cylinder model. Figure 14 shows the LGMAP wire frame representation of the landing gear from various viewing angles. In the figure, the wheel models are black, the oleo and support struts are blue, and the trailing edges are red. Although each of the components are represented by lines in this drawing, their actual diameters are accounted for in the LGMAP prediction.

Figure 15 shows a comparison between the wind-tunnel measurements and the LGMAP prediction. Note that L_p is the one-third-octave sound-pressure-level spectrum (SPL). The experiments and predictions are plotted as continuous lines, with the symbols representing the one-third-octave band values. The contribution from the strut or oleo is predicted quite well, as it should be, because the experimental data were used to calibrate the cylinder element model. The calibrated cylinder coefficients are given in Table 2.

The turbulence Strouhal number and turbulence intensity are used as a starting point for the trailing-edge model, and estimates based on Prandtl's boundary-layer correlations are used for the turbulent thickness and percent plate volume parameters δ and ϵ in the LGMAP trailing-edge model. Depending on the positions of the door relative to other components of the landing gear, the thickness could be fixed by the wake of an upstream component. In this prediction, each acoustic element in LGMAP is assumed to be in the freestream without any interference from other components in the model. Also, in these initial test cases, no reflections from surfaces (such as the aircraft wing) are included. The starting values of the trailing-edge parameters are shown in Table 3.

When calibrating any model, the peak of the reported spectrum and LGMAP prediction are matched first. This sets the values of S_0, C_l, and C_d in the cylinder model and S_0, α, δ, and ϵ in the trailing-edge model. Next, the rise and falloff rates of the function are matched. This sets the values of e and p in both models. Typically, matching the rise and falloff rates changes the peak slightly, and some compromise between peak and falloff rates has to be made.

B. Wheel Element

To calibrate the parameters used in the LGMAP wheel model, the ANOPP wheel noise contribution is used. ANOPP includes only contributions from the oleo or strut and a wheel. Because the ANOPP prediction for the spectrum shape is known to be poor, particularly at higher frequencies, the primary goal of the calibration is to fix the predicted peak level. In the case considered, the aircraft is flying at 120 m at a flight Mach number of 0.2. The landing gear is a four-wheel two-axle full-scale model representative of a Boeing 757 main

Table 3 Parameters used in the trailing-edge model

	e	p	S_0	α	δ	ϵ
Trailing-edge element model	4.0	1.5	1.7	0.1	$0.01 * C$	0.75
Calibrated trailing-edge element model	6.0	3.5	1.9	0.085	$0.15 * C$	0.75

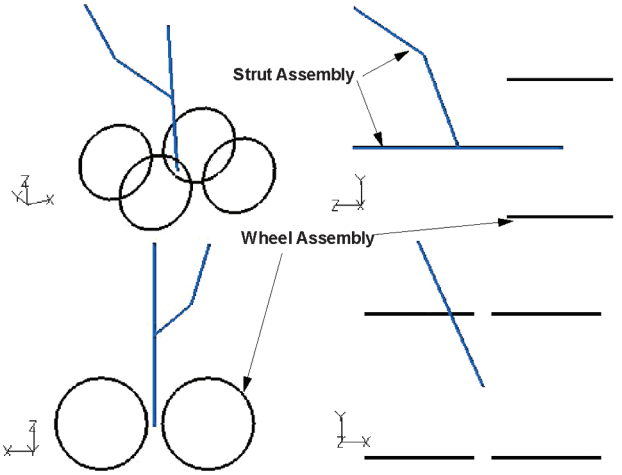

Fig. 16 The LGMAP model for the ANOPP 757 main gear.

landing gear. The simple model of the gear includes only the wheels, the oleo, and the support struts. The LGMAP gear wire frame model is shown in Fig. 16, with the support struts shown in blue and the wheel assemblies in black. The predictions are made for two observer locations: one at a 45 deg polar angle (with the aircraft approaching) and one at a 135 deg (when the aircraft is moving away). The ANOPP and LGMAP predictions are shown in Figs. 17 and 18. It should be noted that LGMAP gives a contribution from the oleo, but it is much lower than the wheel contribution and does not contribute significantly to the total noise. It was found to be difficult to match the very low frequencies exactly. Again, the noise levels are presented as one-third-octave values.

In general, the predictions are quite good. However, because it is recognized that the present wheel model is very crude, no attempt has been made to find the model parameters for the best fit. In addition, as additional acoustic elements are added to the representation of the landing gear, the spectrum shape and levels will certainly change. It should be emphasized that the predictions made here are to provide

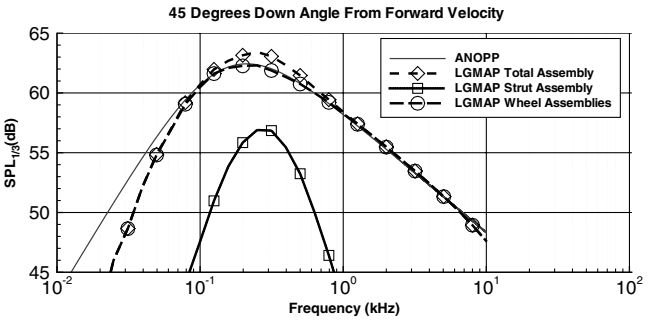

Fig. 17 Comparison between ANOPP and LGMAP predictions for simplified four-wheel landing gear at the aircraft approach microphone.

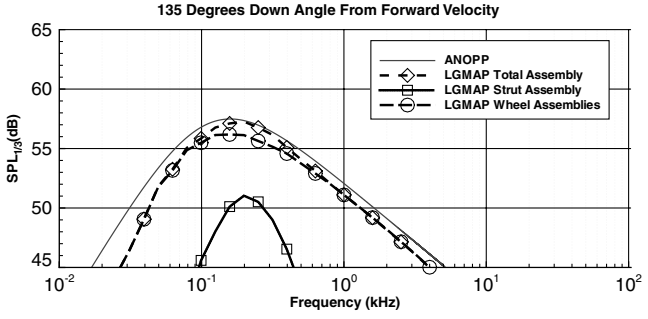

Fig. 18 Comparison between ANOPP and LGMAP predictions for simplified four-wheel landing gear at the aircraft receding microphone.

Table 4 Parameters used in the wheel model

Parameter	Cylinder element model value
e	2.0
p	1.5
S_0	0.18
C_l'	0.34
C_d'	0.17

some confidence that the loading spectrum is realistic. The values of the model parameters for the wheel are shown in Table 4.

IV. Comparisons

In the following subsections, the LGMAP system will be used to predict the noise from three landing-gear configurations. All calibrated coefficients, presented in Sec. III, are kept constant throughout all the predictions. The first comparison is to a Boeing 737 main gear tested in the LSAF [14]. This prediction demonstrates that LGMAP is able to predict the noise from realistic landing-gear geometries. The second comparison will be to the same gear but with increased fidelity. It is shown that LGMAP is able to predict the influence of smaller-scale components on the radiated noise. The final comparison will be to a Boeing 777 main gear tested at Virginia Tech [31].

A. Boeing 737 Undressed Configuration

To assess the effect of adding smaller physical components into the LGMAP representation of landing gear, an example case is considered: a model-scale uninstalled Boeing 737-400 main gear. Noise predictions are compared with the wind-tunnel measurements of Stoker [14]. The test setup, as shown in Fig. 19a, was conducted in the LSAF. These tests compared a dressed 737 main gear without a door to an undressed gear. The primary difference between dressed and undressed landing-gear models was that the dressed configuration included the addition of hoses, as shown in Fig. 19b. All acoustic elements in the preliminary results from LGMAP use the freestream velocity as the local upstream velocity, and there are no acoustic interactions between components.

In Fig. 20a, the LGMAP wire frame representation of the 737-400 undressed model is shown. The support struts are shown in blue, hydraulic brackets are shown in red, and the wheels are shown in black. Each line is representative of the cylinder axis used to model a particular landing-gear component.

LGMAP predictions are compared with the undressed wind-tunnel measurements, with a Mach number of 0.18, 0.20, 0.22, and 0.24, using the same parameters that were determined by calibration

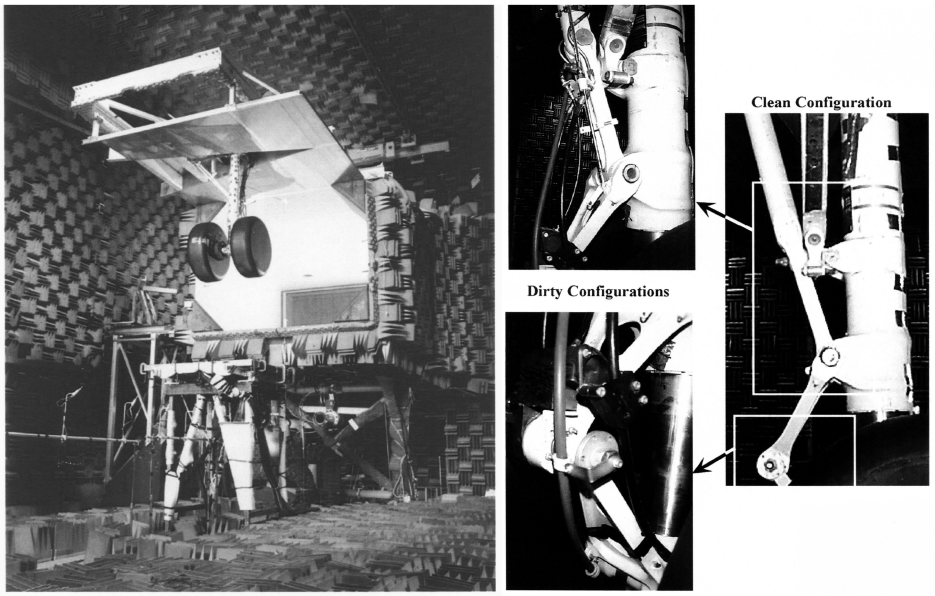

Fig. 19 The test setup of the wind-tunnel results of a Boeing 737-400 main gear at the LSAF (left), and close-up of landing gear with and without dressings (right).

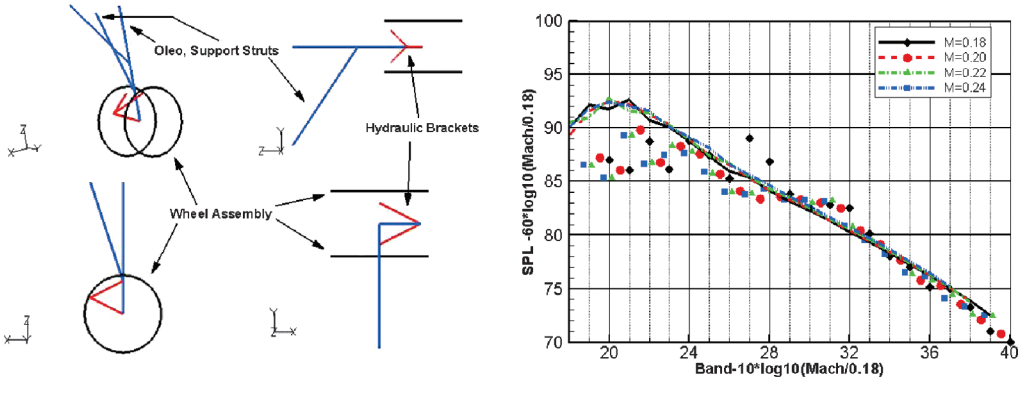

Fig. 20 Diagrams of a) close-up of LGMAP representation of undressed Boeing 737-400 and b) undressed 737-400 landing-gear wind-tunnel measurements (symbols) and LGMAP predictions (lines) for Mach numbers of 0.18, 0.20, 0.22, and 0.24, scaled by V^6.

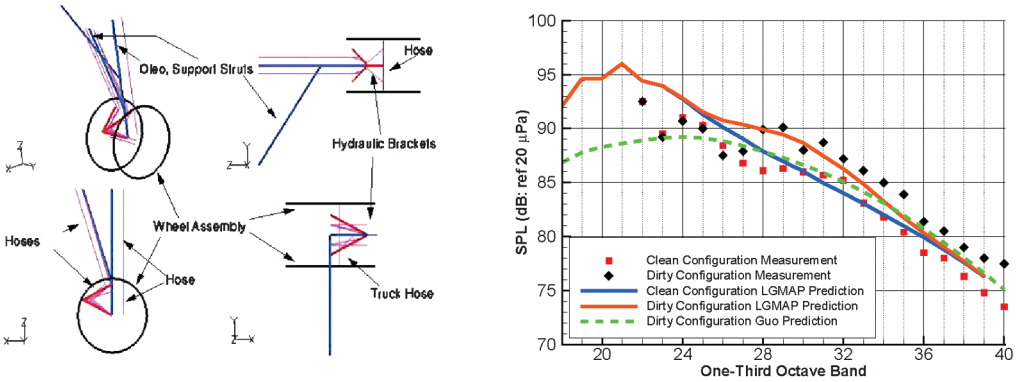

a) b)

Fig. 21 Diagrams of a) four close-up views of the of LGMAP representation of a dressed Boeing 737-400 (support assemblies are blue lines, hydraulic brackets are red lines, wheel assemblies are black lines, and hoses are violet lines) and b) wind-tunnel measurement (symbols) and dressed LGMAP prediction (lines) for Mach number of 0.20.

with the Heller and Dobrzynski [20] DC-10 nose gear and the ANOPP 757 main gear [32]. The noise predictions from LGMAP should scale similar Mach numbers to the sixth power (i.e., V^6). The measurements and predicted values are shown in Fig. 20b (scaled according to Mach number). The agreement between the measurements and predictions is good, except for an anomalous peak in the experimental data at a Mach number of 0.18 in the one-third-octave bands 27 and 28. The source of this discrepancy in the measurements is currently unknown. Also, the difference between prediction and measurement at low frequencies may be due to Reynolds number effects. The undressed LGMAP predictions also collapse to a single line, with the appropriate Mach number scaling, as shown in the figure. The collapse of the predictions is expected, as all the acoustic elements have a sixth-power dependency on velocity.

Even though the LGMAP model for the 737 is only a very approximate representation of the physical geometry, it still provides good agreement throughout the higher frequencies when compared with the measured undressed gear noise. This shows that LGMAP is predicting the general trend of the noise quite satisfactorily. Nevertheless, the current LGMAP model is unable to predict all of the subtle details in the spectrum.

B. Increasing Fidelity in Landing-Gear-Model-and-Acoustic-Prediction Model

Actual landing-gear geometries are not as undressed as the gear used in the measurements shown above. In use, the landing gear will have hoses running along the oleo, the truck, and the other smaller-scale components that generate noise within a certain frequency range. The measurements conducted by Stoker and Sen [16] were for landing gear with and without hoses installed to show how the noise changes when adding smaller components. To demonstrate how LGMAP can predict this change, cylinder models representing these hoses were added and compared with the wind-tunnel experiments.

The LGMAP wire frame representation of the dressed configuration of the 737 is shown in Fig. 21a. Several hoses of various sizes have been added to the undressed configuration to make it a dressed configuration. These include a large hose parallel to the oleo, several small hoses near the support strut, and a hose in wheel truck area. These hoses are approximately in the position of the actual hoses in the experiment, but all of the smooth curves and complexity of the test geometry have not been modeled here. In Fig. 21b, the dressed LGMAP prediction is shown at a Mach number of 0.20 and is compared with both the dressed and undressed 737-400 landing-gear measurements.

The same comparisons are made in Fig. 22 for a range of Mach numbers from 0.18 to 0.24. The addition of the smaller components (hoses) in the LGMAP prediction yields an increment in noise very similar to that measured by Stoker and Sen [16]. At the highest frequencies, the prediction is lower than the measured data, but this may be due to the lack of some of the smallest components or incorrect hose curvature in the LGMAP representation.

C. One-Fourth-Scale Boeing 777 Main Gear

As a final example, a simplified model of a Boeing 777 landing gear is considered. The conditions correspond to the one-fourth-scale model tested in the Virginia Polytechnic Institute and State University Acoustic wind tunnel. The assemblies included in the model are identified in Fig. 23. They are as follows: the strut assembly (including the oleo), the truck assembly, the brake assemblies, the wheels, the aft hydraulic bracket (AHB), the forward

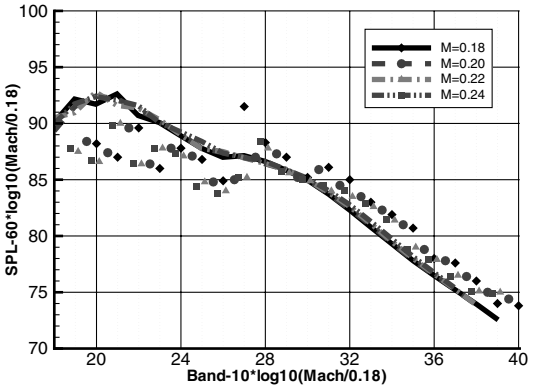

Fig. 22 Dressed wind-tunnel measurement and dressed LGMAP prediction for Mach numbers of 0.18, 0.20, 0.22, and 0.24, scaled by V^6: symbols are wind-tunnel measurements and lines are LGMAP predictions.

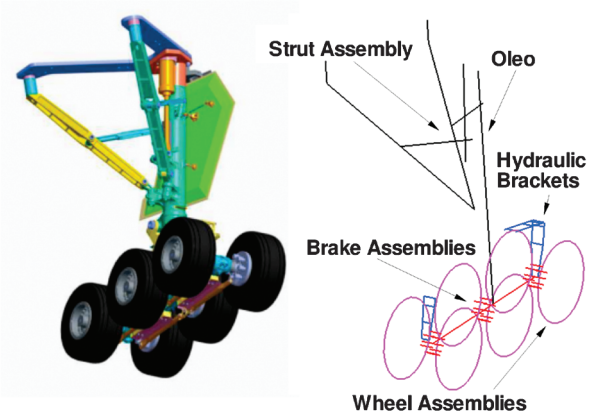

Fig. 23 Wire mesh representation of a Boeing 777 main landing gear, showing the location of the modeled assemblies.

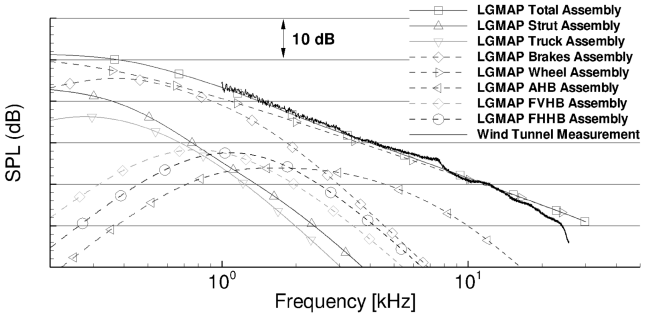

Fig. 24 Comparison of LGMAP results with wind-tunnel measurements for one-fourth-scale Boeing 777 main landing gear. Both total predictions and breakdown by assembly are shown. Predictions are shifted to match measurements at 1 kHz.

vertical hydraulic bracket (FVHB), and the forward horizontal hydraulic bracket (FHHB). Figure 24 shows a comparison of the LGMAP total prediction with the measured data, as well as a breakdown of the noise contributions from the different assemblies. The measurements and the predictions are both for a 6.25 Hz constant bandwidth, and the measurements are averaged values from an overhead microphone array. Although the general shape of the predicted spectrum is reasonable (the measured data are not shown below 1 kHz because of probable tunnel noise contamination), the level is not shown because the reported wind-tunnel measurement levels are suspect. However, to match the spectrum shape, the predictions were shifted to match the levels at 1 kHz.

From the predicted breakdown of the assembly contributions to the noise, the largest noise sources (at the overhead location) are the wheel assemblies. At the lower frequencies, the brake and strut assemblies begin to influence the total noise signature and, at the higher frequencies, the hydraulic brakes are also influencing factors to the total noise. Although the discrepancy in the predicted amplitude remains to be resolved, the predictions in this section should serve to indicate the manner in which the LGMAP methodology will work in the future.

V. Conclusions

The initial framework for the prediction of noise from complex geometry landing gear using a toolkit made of simple acoustic elements has been presented. The simple acoustic elements include cylinders with a modeled shedding frequency spectrum, both physics and empirically based. The majority of components on the landing gear are modeled as cylinders, and the wheels are represented by a ring of cylinders. Each cylinder then generates noise in a frequency range dependent on its shape and local flow. The method is still in an early stage of development, and many new features need to be implemented, including flow and acoustic effects on the radiated noise; however, it has been demonstrated that this method, even in its early stage in development, can predict the radiated noise of the complete structure at certain observer positions.

The framework shown is much more robust than a fully empirical model, such as ANOPP, and is many orders of magnitude less expensive in time and computer cost than a full numerical calculation using CFD. Unlike any previous prediction system, it is also object-oriented to allow for expansion and improvement over time, as well as separable enough to allow for component acoustic analysis to identify those components generating the most significant noise. These features will significantly help in the design of future landing-gear geometries.

It is expected that the fidelity and accuracy of the acoustic elements will evolve over time: initially described by simple acoustic models, validated by comparison with experiments and flight data, and followed by revisions and refinements. This framework is based on the assumption that a full numerical simulation will be impractical if not impossible to achieve. As further geometric details, additional source mechanisms (such as trailing-edge scattering), or acoustic effects (such as shielding) are predicted, the execution time for the code will increase. However, it is certain to be orders of magnitude less computationally expensive than a direct noise calculation and orders of magnitude less expensive in cost than an experiment.

Acknowledgment

This study was supported by NASA Langley Research Center under NASA grant NAG1-03025, with technical officer David Lockard.

References

[1] "Noise Standards: Aircraft Type and Airworthiness Certification," *Federal Aviation Regulations*, Pt. 36, Federal Aviation Administration, June 1974; reprint, Federal Aviation Administration, 12 Aug. 1985.

[2] Ginevsky, A. S., Vlasov, Y. V., and Karavosov, R. K., *Acoustic Control of Turbulent Jets*, Springer–Verlag, New York, 2004.

[3] Lasagna, P. L., Mackall, K. G., Burcham, F. W., Jr., and Putnam, T. W., "Landing Approach Airframe Noise Measurements and Analysis," NASA TP-1602, Jan. 1980.

[4] Liebeck, R. H., "Design of the Blended Wing Body Subsonic Transport," *Journal of Aircraft*, Vol. 41, No. 1, 2004, pp. 10–25. doi:10.2514/1.9084

[5] Nark, D. M., Burley, C. L., Tinetti, A., and Rawls, J. W., Jr., "Initial Integration of Noise Prediction Tools for Acoustic Scattering Effects," AIAA Paper 2008-2996, 2008.

[6] Crighton, D. G., *Airframe Noise*, Acoustical Society of America, Woodbury, NY, 1995.

[7] Lilley, G. M., "The Prediction of Airframe Noise and Comparison with Experiment," *Journal of Sound and Vibration*, Vol. 239, No. 4, 2001, pp. 849–859. doi:10.1006/jsvi.2000.3219

[8] Fink, M. R., "Noise Component Method for Airframe Noise," *Journal of Aircraft*, Vol. 16, No. 10, 1979, pp. 659–665. doi:10.2514/3.58586

[9] Ffowcs Williams, J. E., and Hall, L. H., "Aerodynamic Sound Generation by Turbulent Flow in the Vicinity of a Scattering Half-Plane," *Journal of Fluid Mechanics*, Vol. 40, 1970, pp. 657–670. doi:10.1017/S0022112070000368

[10] Hardin, J. C., "Noise Radiation from the Side Edges of Flaps," *AIAA Journal*, Vol. 18, No. 5, May 1980, pp. 549–552. doi:10.2514/3.7668

[11] Brooks, T. F., Pope, S. D., and Marcolini, M. A., "Airfoil Self-Noise and Prediction," NASA RP-1218, July 1989.

[12] Guo, Y., "Airframe Noise Prediction by Acoustic Analogy," NASA Langley Research Center NAS1-00086, Hampton, VA , Feb. 2004.

[13] Guo, Y., "A Study on Local Flow Variations for Landing Gear Noise Research," AIAA Paper 2008-2915, 2008.

[14] Stoker, R. W., "Landing Gear Noise Test Report," NASA NAS1-97040, 1999.

[15] Kipersztok, O., and Senguptat, G., "Flight Test of the 747-JT9D for Airframe Noise," *Journal of Aircraft*, Vol. 19, No. 12, 1982, pp. 1061–1069. doi:10.2514/3.44812

[16] Stoker, R. W., and Sen, R., "An Experimental Investigation of Airframe Noise Using a Model-Scale Boeing 777," AIAA Paper 2001-0987, 2001.

[17] Lockard, D. P., Khorrami, M. R., and Li, F., "High Resolution Calculation of a Simplified Landing Gear," AIAA Paper 2004-2887, 2004.

[18] Zorumski, W. E., "Aircraft Noise Prediction Program. Theoretical Manual: Parts 1 and 2," NASA TM-83199, 1982.

[19] Fink, M. R., "Component Method for Airframe Noise," Federal Aviation Administration, TR FAA-RD-77-29, 1977.

[20] Heller, H. H., and Dobrzynski, W. M., "Sound Radiation from Aircraft Wheel-Well/Landing-Gear Configurations," *Journal of Aircraft*, Vol. 14, No. 8, 1977, pp. 768–774. doi:10.2514/3.58851

[21] Guo, Y. P., Yamamoto, K. J., and Stoker, R. W., "Experimental Study on Aircraft Landing Gear Noise," *Journal of Aircraft*, Vol. 43, No. 2, 2006, pp. 306–317. doi:10.2514/1.11085

[22] Lopes, L. V., Brentner, K. S., and Morris, P. J., "Airframe Noise Prediction with Installed Landing Gear for a Complete Aircraft," AIAA Paper 2009-3155, 2009.

[23] Zdravkovich, M. M., *Flow Around Circular Cylinders, Fundamentals*, Vol. 1, Oxford Univ. Press, New York, 1997.

[24] Zdravkovich, M. M., *Flow Around Circular Cylinders, Applications*, Vol. 2, Oxford Univ. Press, New York, 2003.
[25] Howe, M. S., "A Review of the Theory of Trailing Edge Noise," *Journal of Sound and Vibration*, Vol. 61, No. 3, 1978, pp. 437–465. doi:10.1016/0022-460X(78)90391-7
[26] Howe, M. S., "Trailing Edge Noise at Low Mach Numbers," *Journal of Sound and Vibration*, Vol. 225, No. 2, 1999, pp. 211–238. doi:10.1006/jsvi.1999.2236
[27] Howe, M. S., "Trailing Edge Noise at Low Mach Numbers, Part 2: Attached and Separated Edge Flows," *Journal of Sound and Vibration*, Vol. 234, No. 5, 2000, pp. 761–775. doi:10.1006/jsvi.1999.2861
[28] Brès, G. A., Brentner, K. S., Perez, G., and Jones, H. E., "Maneuvering Rotorcraft Noise Prediction," *Journal of Sound and Vibration*, Vol. 275, Nos. 3–5, Aug. 2004, pp. 719–738. doi:10.1016/j.jsv.2003.07.005
[29] Brentner, K. S., Lopes, L. V., Chen, H. N., and Horn, J. F., "Near Real-Time Simulation of Rotorcraft Acoustics and Flight Dynamics," *Proceedings of the American Helicopter Society 59th Annual Forum*, AHS International, Alexandria, VA, 2003.
[30] Ffowcs Williams, J. E., and Hawkings, D. L., "Sound Generated by Turbulence and Surfaces in Arbitrary Motion," *Philosophical Transactions of the Royal Society of London. Series A, Mathematical and Physical Sciences*, Vol. 264, No. 1151, 1969, pp. 321–342. doi:10.1098/rsta.1969.0031
[31] Ravetta, T. A., Burdisso, R. A., and Ng, W. F., "Wind Tunnel Aeroacoustic Measurements of a 26%-Scale 777 Main Landing Gear Model," AIAA Paper 2002-2885, 2004.
[32] Lopes, L. V., Brentner, K. S., Morris, P. J., Lilley, G. M., and Lockard, D. P., "Complex Landing Gear Noise Using a Simple Toolkit," AIAA Paper 2005-1202, 2005.